Int. J. Environ. Sci. Technol. (2016) 13:1973–1988
DOI 10.1007/s13762-016-1022-3

ORIGINAL PAPER

Heavy metal biosorption potential of a Malaysian Rhodophyte (*Eucheuma denticulatum*) from aqueous solutions

Md. S. Rahman[1] · K. V. Sathasivam[1]

Received: 12 February 2016 / Revised: 4 May 2016 / Accepted: 18 May 2016 / Published online: 2 June 2016

Abstract Biosorption is a promising technology for the removal of heavy metals from industrial wastes and effluents. In the present study, biosorption of Pb^{2+}, Cu^{2+}, Fe^{2+} and Zn^{2+} onto the dried biomass of *Eucheuma denticulatum* (Rhodophyte) was investigated as a function of solution pH, contact time, temperature and initial metal ion concentration. The experimental data were evaluated by Langmuir, Freundlich, Temkin and Dubinin–Radushkevich isotherm models. The sorption isotherm data followed Langmuir and Freundlich models, and the maximum Langmuir monolayer biosorption capacity was found as 81.97, 66.23, 51.02 and 43.48 mg g^{-1} for Pb^{2+}, Cu^{2+}, Fe^{2+} and Zn^{2+}, respectively. The sorption kinetic data followed pseudo-second-order and intraparticle diffusion models. Thermodynamic study revealed feasible, spontaneous and endothermic nature of the sorption process. Fourier transform infrared analysis showed the presence of amine, aliphatic, carboxylate, carboxyl, sulfonate and ether groups in the cell wall matrix involved in metal biosorption process. A total of nine error functions were applied in order to evaluate the best-fitting models. We strongly suggest the analysis of error functions for evaluating the fitness of the isotherm and kinetic models. The present work shows that *E. denticulatum* can be a promising low-cost biosorbent for removal of the experimental heavy metals from aqueous solutions. Further study is warranted to evaluate its potential for the removal of heavy metals from the real environment.

✉ K. V. Sathasivam
kathir.aimst@gmail.com

[1] Faculty of Applied Sciences, AIMST University, Jalan Semeling-Bedong, 08100 Bedong, Kedah, Malaysia

Keywords *Eucheuma denticulatum* · Biosorption · Heavy metals · Fourier transform infrared · Error functions · Malaysia

Introduction

Due to the growing demand of the world's increasing population, industrialization has been intensified over the world. Every industrial processing plant results in some sorts of wastes that find their way into the water systems (Grassi et al. 2012). Heavy metals are released into the aquatic environment from several domestic (automobile exhaust, smelting processes, burning of fossil fuels, incineration of wastes, landfill leaches, use of sewage sludge, municipal wastewater, urban runoff) and industrial processes like electroplating, refining ore, mining, electronic and metal-finishing industries, fertilizer industry, tanneries, painting, paper industries and pesticides (Gautam et al. 2015). Heavy metals of industrial effluents have become global environmental and public health concern due to their toxicities, non-biodegradability, bioaccumulation in human body and food chain, carcinogenicities and mutagenesis in various living organisms (Sarkar et al. 2014; Chowdhury et al. 2015).

Numerous methods such as chemical precipitation, ion exchange, coagulation–flocculation, flotation, membrane filtration, electrochemical treatment, magnetic separation and purification, biosorption and nanotechnology are being used for the treatment and removal of heavy metals from water and wastewater (Gautam et al. 2015). Among them, biosorption process has been regarded as a promising cost-effective, sustainable and eco-friendly technology (He and Chen 2014). This process offers a number of advantages in comparison with the conventional methods (Macek and Mackova 2011). A wide range of commercial and

potentially low-cost adsorbents including living or dead microorganisms, seaweeds, plant materials, industrial and agricultural wastes, natural residues, and inorganic precursors including red mud, clays, blast furnace slags, zeolites, chitosan and peat has been reported in the literature (Bilal et al. 2013; Grassi et al. 2012; Macek and Mackova 2011).

Seaweeds are widely distributed in marine, freshwater as well as terrestrial ecosystems, which can serve as good biosorbents due to their abundance, cost-effectiveness, reusability and high metal sorption capacities (Bilal et al. 2013; He and Chen 2014). Despite the fact that the red algae constitute carrageenan that provides different binding sites (e.g., hydroxyl, carboxyl, amino and sulfhydryl) responsible for the adsorption for heavy metals (Grassi et al. 2012), they are the least focused group (Rathod et al. 2014). Therefore, further research is warranted on the selectivity of algal species for their use as a low-cost biosorbent (Grassi et al. 2012).

The red seaweed, *Eucheuma denticulatum,* is one of the most important commercial sources of iota-carrageenan (Freile-Pelegrín et al. 2006), which also has different nutritional values (Renaud and Luong-Van 2006). This species has an interesting phytoremediation capacity in treating contaminated waters (Perales and Leysa 2012). However, there is no available literature report on the biosorption of heavy metals using the dried biomass of *E. denticulatum*. Hence, the present study was investigated to evaluate the seaweed in the removal of Pb^{2+}, Cu^{2+}, Fe^{2+} and Zn^{2+} from aqueous solutions in batch system at laboratory scale under different parameters like solution pH, contact time, temperature and initial metal ion concentrations. The Fourier transform infrared (FTIR) spectroscopy study was made to identify the main functional groups involved in the biosorption process of those metal ions.

In general, mechanistic or empirical equations are used to express heavy metal adsorption capacities of different types of biosorbents using batch or column method (Park et al. 2010). Nearly two dozens of empirical models involving 2, 3, 4 or even 5 parameters have been used to fit batch equilibrium isotherm curves to biosorbents (Basha et al. 2010; Park et al. 2010). Besides, kinetic models have been described by several authors elsewhere (Plazinski and Plazinska 2012; Gupta and Bhattacharyya 2011). The equilibrium and kinetic models are often validated on the basis of coefficient of regression ($R^2 \geq 0.99$) of the experimental data. However, the use of R^2 is inappropriate for comparing the best-fitting models since this parameter fails to represent the error for fitting with linear equation (Ho 2004). Hence, the use of more than one error has been suggested to describe the validity of adsorption models (Ncibi et al. 2008). In recent years, more than single error function of nonlinear regression has been used to determine the best-fitting models (Chan et al. 2012; Subramanyam and Das 2014; Sreńscek-Nazzal et al. 2015; Kumar et al. 2016). In the present study, nine error functions were used in order to evaluate the best-fitting models. The present study was carried out in the Biotechnology Research Laboratory of the AIMST University, Malaysia, during the period of May to October 2014.

Materials and methods

Collection, identification and preparation of the biosorbent

The red seaweed *E. alvarezii* was collected from the Semporna coast of Sabah, Malaysia, in April 2013. The thallus of the seaweed was washed for several times with running water and subsequently with deionized water to remove epiphytes and salts. The washed biomass was then dried in an oven at 60 °C for 48 h until a constant weight was attained. The dried biomass was then crushed with an analytical mill, sieved (250 µm size) and stored in polypropylene bottles until use.

The living biomass of the species was preliminarily identified following systemic morphological features (Carpenter and Niem 1998). It was then subjected to 28S DNA-based molecular identification (Sherwood et al. 2010). The species was identified as *E. denticulatum,* and the gene sequence of the nucleotide was submitted in the NCBI GenBank (accession number KM229319).

Chemicals and reagents

All the chemicals and reagents used in this study were of analytical reagent grade. The working solutions of different concentrations (10–200 mg L^{-1}) of the heavy metals (Pb, Cu, Fe and Zn) were prepared by diluting the stand solutions (1000 ± 2 mg L^{-1}) of the respective metals (Merck, Germany) in double-distilled deionized water. Different initial pH of the solutions was obtained by adding 0.1 N HCl (Sigma-Aldrich, USA) or 0.1 N NaOH (Merck, Germany).

Batch biosorption experiments

All the experiments were conducted in a batch system using 150-mL Erlenmeyer flasks in a thermostatic shaker (25 °C, 180 rpm), unless otherwise stated. Each flask was filled with 50 mL of solution and biosorbent as appropriate. The influence of the operational parameters such as solution pH (2–7), contact time (0–120 min), initial metal ion concentration (25–200 mg L^{-1}) and temperature (25–50 °C) on the biosorption characteristics of the metals

was assessed using a constant biomass dosage (4 mg L^{-1}). Competitive adsorption of the four metal ions under mixed condition was also evaluated.

The amount of the metal ions remaining in the solutions were measured spectrophotometrically by using Atomic Absorption Spectrometer (AAnalyst700, PerkinElmer, USA) after the separation of biosorbent by filtration through Whatman Filter No. 1.

The sorption kinetics studies were conducted with 50 mL of the metal solutions at an initial concentration of 10 mg L^{-1}. The sample solutions were withdrawn at regular intervals, and the residual concentration of the heavy metals in the aqueous phase was analyzed after filtration as stated above.

Biosorption capacity

The amount of metal adsorbed per gram of the biosorbent at equilibrium, q_e (mg g^{-1}), was calculated from the difference of the metal concentration in the aqueous phase before and after biosorption as follows:

$$q_e = \frac{(C_0 - C_e) \times V}{m} \quad (1)$$

where C_0 and C_e are the initial and equilibrium concentration of metal ions in the solution (mg L^{-1}), respectively, V is the volume of metal solution (L), and m is the mass of the dry biosorbent (g).

The percentage of metal removal (R, %) from the solution was calculated as follows:

$$R\,(\%) = \frac{(C_0 - C_e) \times 100}{C_0} \quad (2)$$

Isotherm models

In the present experiment, four two-parameter isotherm models (Langmuir, Freundlich, Temkin and Dubinin–Radushkevich) in their linear forms were applied to describe the sorption behavior of the adsorbent. Parameters of the isotherm models are given in Table 1.

Kinetic models

The metal ions adsorption on the biosorbent was analyzed by using linearized form of four kinetic models: pseudo-first-order, pseudo-second-order, Elovich and intraparticle diffusion models. Parameters of the kinetic models are shown in Table 1.

Thermodynamic study

The chemical thermodynamics of reactions is described by using three 'thermodynamic potentials,' i.e., internal energy (entropy), enthalpy and the Gibbs free energy. These thermodynamic parameters were calculated to determine the feasibility and nature of the biosorption of the experimental metal ions onto the adsorbent. Parameters of the thermodynamic study are given in Table 1.

Error function analysis

In order to evaluate the suitability of the equation to the experimental data error function is the best optimization procedure. Apart from the regression coefficient (R^2), nine error functions (such as sum of square error, SSE; average relative error, ARE; hybrid functional error, HYBRID; sum of absolute error, EABS; Marquardt's percent standard deviation, MPSD; normalized standard deviation, Δq (%); coefficient of determination, r^2; nonlinear Chi-square test, χ^2; and residual root-mean-square error, RMSE) were calculated to test the fitness of the models (Table 2).

Statistical analysis

Each typical experiment was done in triplicate, and the data were expressed as the mean of the triplicate results. Necessary statistical analyses were performed using Microsoft Office Excel 2007 (Microsoft Corp., USA).

Fourier transform infrared spectroscopy (FTIR)

Infrared spectra of the raw and metal-loaded biomass were obtained using a Fourier transform infrared spectrometer (Spectrum GX, PerkinElmer, USA). The FTIR spectra were recorded using a PerkinElmer spectrometer over the wave number range 400–4000 cm^{-1} with 10 scans at a resolution of 4 cm^{-1} under ambient conditions.

Results and discussion

Effect of solution pH

In the adsorption process of metal ions from aqueous solutions, pH of the solution plays an important role. Biosorption increased gradually with the increase in pH (Fig. 1a). The maximum biosorption (90.47 % for Pb^{2+}, 66.95 % for Cu^{2+}, 60.99 % for Fe^{2+} and 45.51 % for Zn^{2+}) was observed at pH 5. At lower pH (2–4), biosorption of metal ions was inhibited greatly. At low pH, the functional groups (as described in the FTIR section) are positively charged because of high H^+ concentration, which increased competition between protons and metal cations for binding active sites of biomass, resulting in decreasing the metal cations adsorption on the biomass surfaces (Yalçın 2014).

Table 1 Isotherm, kinetic and thermodynamic model parameters used in the study

Model	Parameters		References
Isotherm models			
Langmuir	$\frac{C_e}{q_e} = \frac{1}{K_L q_m} + \frac{C_e}{q_m}$	(3)	Langmuir (1918)
	$R_L = \frac{1}{(1+K_L C_0)}$	(4)	Weber and Chakravorti (1974)
Freundlich	$\log q_e = \log K_F + \frac{1}{n}\log C_e$	(5)	Freundlich (1906)
Temkin	$q_e = \left(\frac{R_T}{b_T}\right)\ln A_T + \left(\frac{R_T}{b_T}\right)C_e$	(6)	Temkin and Pyzhev (1940)
D–R	$\ln(q_e) = \ln(q_m) - B_D\varepsilon^2$	(7)	Dubinin and Radushkevich (1947)
	$\varepsilon = RT\ln\left(1+\frac{1}{C_e}\right)$	(8)	
	$E = \frac{1}{\sqrt{(-2B_D)}}$	(9)	Hobson (1969)
Kinetic models			
Pseudo-first-order	$\log(q_e - q_t) = \log q_e - \frac{k_1 t}{2.303}$	(10)	Lagergren (1898)
Pseudo-second-order	$\frac{t}{q_t} = \frac{1}{k_2 q_e^2} + \frac{t}{q_e}$	(11)	Ho (1995)
	$h = k_2 q_e^2$	(12)	
	$t_{1/2} = \frac{1}{k_2 q_e}$	(13)	
Elovich	$\frac{dq_t}{d_t} = \alpha\exp(-\beta q_t)$	(14)	Roginsky and Zeldovich (1934)
	$q_t = \frac{1}{\beta}\ln(\alpha\beta) + \frac{1}{\beta}\ln(t)$	(15)	Chien and Clayton (1980)
Intraparticle diffusion	$q_t = k_d t^{0.5} + C$	(16)	Weber and Morris (1963)
	$F = 1 - \frac{6}{\pi^2}\sum\frac{1}{N^2}\exp(-N^2 B_t)$	(17)	Boyd et al. (1947)
	$F = \frac{q_t}{q_e}$	(18)	
	$t_{1/2} = 0.03\frac{r^2}{D_i}$	(19)	Su et al. (2013)
	$B_t = -0.4977 - \ln(1-F)$	(20)	Reichenberg (1953)
Thermodynamic model			
Gibbs free energy	$\Delta G^\circ = -RT\ln K_{eq}$	(21)	Gibbs (1873)
	$\Delta G^\circ = \Delta H^\circ - T\Delta S^\circ$	(22)	
	$\ln K_{eq} = \frac{\Delta S^\circ}{R} - \frac{\Delta H^\circ}{RT}$	(23)	
	$K_{eq} = \frac{q_e}{C_e}$	(24)	

C_0 (mg L^{-1}) is the adsorbate initial concentration, C_e (mg L^{-1}) is the equilibrium concentration, q_e (mg g^{-1}) is the observed biosorption capacity at equilibrium, q_m (mg g^{-1}) is the maximum biosorption capacity, R_L is the dimensionless constant, known as separation factor, K_L (L mg^{-1}) is a Langmuir constant related to the energy of adsorption, K_F (mg g^{-1}) (L $mg^{-1})^{1/n}$ is the Freundlich isotherm constant related to the sorption capacity, n is the constant which gives an idea of the grade of heterogeneity, R (8.314 J mol^{-1}) is the universal gas constant, A_T (L mg^{-1}) is the equilibrium binding constant corresponding to the maximum binding energy, b_T (J mol^{-1}) is the Temkin constant related to heat of sorption, B_D (mol^2 kJ^{-2}) is D–R isotherm constant which expresses the mean biosorption energy, ε is the Polanyi potential related to the equilibrium concentration, T (K) is the absolute temperature, E (kJ mol^{-1}) is the mean of free energy, q_t (mg g^{-1}) is the adsorption capacity at time t, k_1 (min^{-1}) is the pseudo-first-order rate constant of adsorption, k_2 (g mg^{-1} min^{-1}) is the equilibrium pseudo-second-order rate constant of sorption, h (mg g^{-1} min^{-1}) is the initial adsorption rate, $t_{1/2}$ (min) is the half-adsorption time, α (mg g^{-1} min^{-1}) is the initial adsorption rate constant, β (g mg^{-1}) is the desorption constant, C (mg g^{-1}) is the boundary layer diffusion effect, k_d (mg g^{-1} $min^{-0.5}$) is the rate constant for intraparticle diffusion, B (min^{-1}) is the Boyd's constant, F is the fractional attainment of equilibrium at time t, N is an integer that defines the infinite series solution, r (cm) is the radius of the particle, D_i (cm^2 s^{-1}) is the diffusion coefficient, $\Delta G°$ (kJ mol^{-1}) is the change in Gibbs free energy, $\Delta H°$ (kJ mol^{-1}) is the change in enthalpy, $\Delta S°$ (kJ mol^{-1} K^{-1}) is the change in entropy, K_{eq} is the thermodynamic equilibrium constant

As the pH increases, the acidic dissociation of several functional groups on the adsorbent surface could take place which is dependent of the acid dissociation constant (pK_a) values of each group. At $pH < pK_a$, the neutral functional groups restrict the metal cations access to the sorbent active sites due to repulsive forces. Conversely, at $pH > pK_a$, negatively charged functional groups reduce the electrostatic repulsions allowing the bonding of metal cations and

Table 2 Equations of the error functions used in the study

Error function		References
$\mathrm{SSE} = \sum_{i=1}^{n} \left(q_{\mathrm{e,calc}} - q_{\mathrm{e,exp}}\right)^2$	(25)	Subramanyam and Das (2014)
$\mathrm{ARE} = \frac{100}{N} \sum_{i=1}^{n} \left\lvert q_{\mathrm{e,exp}} - q_{e,\mathrm{calc}} \right\rvert$	(26)	Subramanyam and Das (2014)
$\mathrm{HYBRID} = \frac{100}{(N-P)} \sum_{i=1}^{n} \frac{\left(q_{\mathrm{e,exp}} - q_{e,\mathrm{calc}}\right)}{q_{\mathrm{e,exp}}}$	(27)	Subramanyam and Das (2014)
$\mathrm{EABS} = \sum_{i=1}^{n} \left\lvert q_{\mathrm{e,exp}} - q_{\mathrm{e,calc}} \right\rvert$	(28)	Subramanyam and Das (2014)
$\mathrm{MPSD} = 100 \sqrt{\left(\frac{1}{N-P}\right) \sum_{i=1}^{n} \left(\frac{q_{\mathrm{e,exp}} - q_{\mathrm{e,calc}}}{q_{\mathrm{e,exp}}}\right)^2}$	(29)	Subramanyam and Das (2014)
$\Delta q(\%) = 100 \sqrt{\frac{1}{N-1} \sum_{i=1}^{n} \left(\frac{q_{\mathrm{e,exp}} - q_{\mathrm{e,calc}}}{q_{\mathrm{e,exp}}}\right)^2}$	(30)	Wang et al. (2010)
$r^2 = \frac{\sum_{i=1}^{n} \left(q_{\mathrm{e,calc}} - \overline{q_{\mathrm{e,exp}}}\right)^2}{\sum_{i=1}^{n} \left(q_{\mathrm{e,calc}} - \overline{q_{\mathrm{e,exp}}}\right)^2 + \sum_{i=1}^{n} \left(q_{\mathrm{e,calc}} - q_{\mathrm{e,exp}}\right)^2}$	(31)	He et al. (2010)
$\chi^2 = \sum_{i=1}^{n} \frac{\left(q_{\mathrm{e,exp}} - q_{\mathrm{e,calc}}\right)^2}{q_{\mathrm{e,calc}}}$	(32)	Ho and Ofomaja (2006)
$\mathrm{RMSE} = \sqrt{\frac{1}{N-2} \sum_{i=1}^{n} \left(q_{\mathrm{e,exp}} - q_{\mathrm{e,calc}}\right)^2}$	(33)	Vijayaraghavan et al. (2006)

$q_{\mathrm{e,exp}}$ (mg g^{-1}) is the value obtained from the batch experiment, $q_{\mathrm{e,calc}}$ (mg g^{-1}) is the calculated value from the isotherm for corresponding $q_{\mathrm{e,exp}}$, $\overline{q_{\mathrm{e,exp}}}$ (mg g^{-1}) is the mean of $q_{\mathrm{e,exp}}$, N is the number of observations in the experimental isotherm, and P is number of parameters in the respective model

increasing the metal removal (de Souza et al. 2013). As the adsorbent surfaces become more negatively charged with the increase of pH, it facilitates the uptake of the metal cations through surface complexation or electrostatic interaction (Yalçın 2014). Therefore, all the rest biosorption experiments were carried out at pH 5.

Effect of contact time

Biosorption of metal ions on the adsorbent increased with an increase in contact time (Fig. 1b). More than 75 % of the total adsorption was attained within 30 min. The rapid kinetic mechanism can be attributed to the formation of exterior surface complexes neglecting intraparticle diffusion, which is very advantageous in biotechnological processes for wastewater treatment (Yalçın 2014). The biosorption process becomes slow during the later stage incubation indicating the maximum adsorption level as a saturation point of biosorption ($\sim$120 min) as the free available surfaces for adsorption become occupied (Al-Homaidan et al. 2014; Ibrahim 2011). Hence, a contact time of 120 min was selected for further experiments.

Effect of initial concentration of metal ions

The biosorption capacity of the biomass increased with increasing initial concentration of the metal ions (Fig. 1c), which can be attributed to an increase in electrostatic interactions involving sites of progressively lower affinity for the metal ions up to the point of saturation (Arshadi et al. 2014; Meitei and Prasad 2014). Conversely, the percentage removal of the metal ions decreased markedly in the range of 73.04–63.71, 66.48–55.12, 62.88–49.02 and 54.56–40.87 % for Pb^{2+}, Cu^{2+}, Fe^{2+} and Zn^{2+}, respectively, with an increase in the initial concentration of the metal ions from 0 to 200 mg L^{-1}. This phenomenon might be due to the rapid saturation of all metal-binding active sites of the biosorbent at a certain concentration of the metal ions (Al-Homaidan et al. 2014; Meitei and Prasad, 2014).

Effect of temperature

As shown in Fig. 1d, biosorption of metal ions increased with the increase of solution temperature. The uptake of Pb^{2+}, Cu^{2+}, Fe^{2+} and Zn^{2+} by the sorbent increased in the range of 90.47–94.8, 66.95–69.92, 60.99–66.17 and 45.51–51.85 %, respectively, with an increase in temperature from 298 to 323 °K. It can be attributed that at the higher temperatures, the activation of the biosorbent surfaces is enlarged facilitating more active sites for biosorption of the metal ions. Moreover, an easy mobility and enhanced accessibility of metal ions from the bulk solution to the biomass active sites could also be the

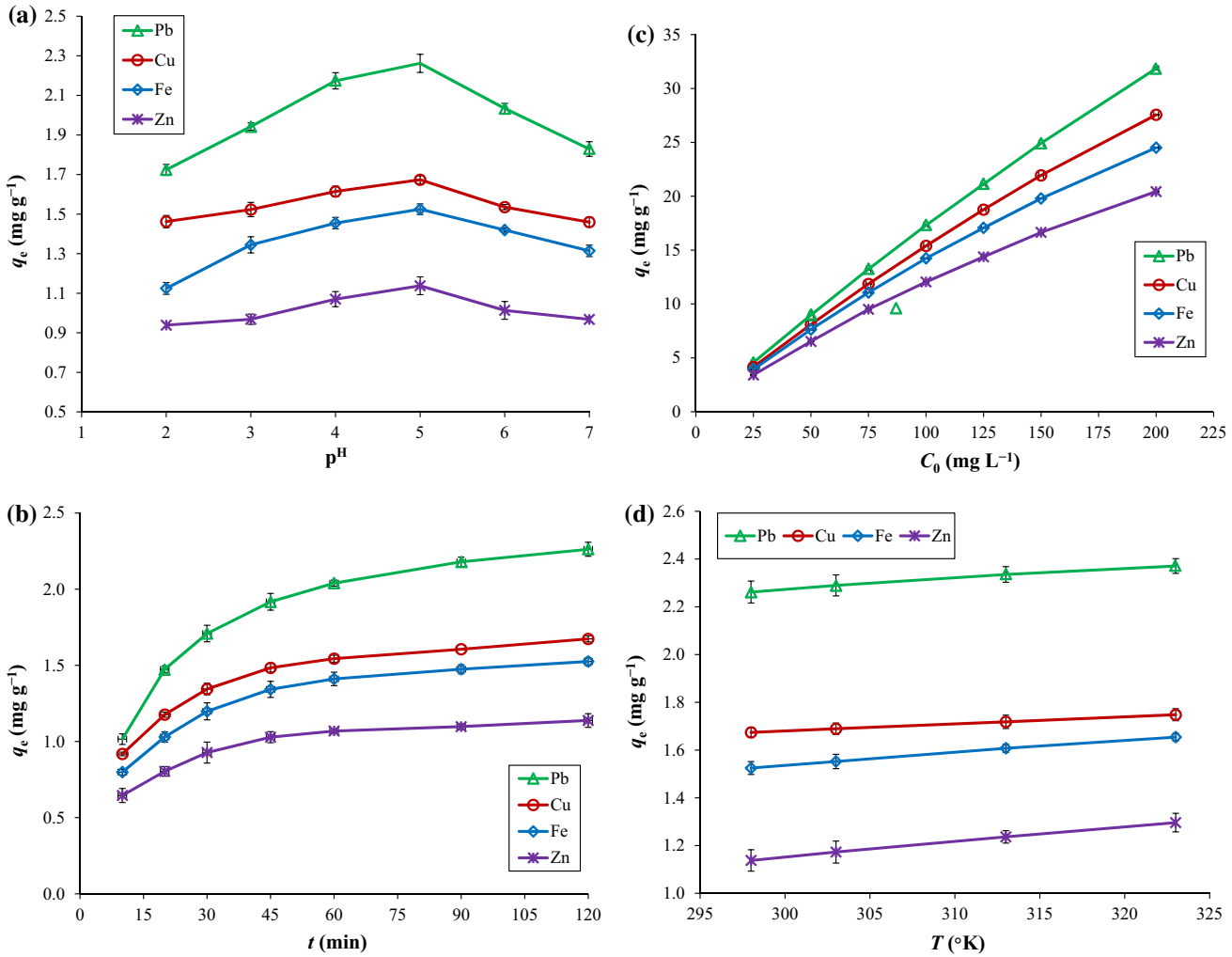

Fig. 1 Effect of different parameters on the metal ions biosorption onto *E. denticulatum*: **a** solution pH, **b** contact time, **c** initial metal ions concentration and **d** temperature

possible reason for the maximum biosorption of metal ions at higher temperatures (Arshadi et al. 2014).

Biosorption studies

The equilibrium adsorption isotherms are essential data source to design, understand and optimize the biosorption process. In the present study, the experimental equilibrium data were explained using Langmuir, Freundlich, Temkin and Dubinin–Radushkevich (D–R) isotherm models.

Langmuir isotherm model

As shown in Fig. 2a, approximately linear relationship ($R^2 \geq 0.99$) was observed in the Langmuir adsorption isotherm. The maximum Langmuir monolayer adsorption capacity, q_m (mg g^{-1}), as shown in Table 3, was found to increase in the following order: Pb^{2+} (81.97) > Cu^{2+} (66.23) > Fe^{2+} (51.02) > Zn^{2+} (43.48) suggesting that the Pb^{2+} has a preferential uptake compared to the other metals, which can be attributed to its low tendency in forming strong complex (Lasheen et al. 2012). Another reason might be attributed to carboxylate polysaccharides representing in the biomass that show preferential binding of cations with large ionic radii (Yalçın 2014). However, the preferential sorption order of the metal ions in the present study could be explained by Pauling's electronegativity (Pauling 1960): Pb^{2+} (2.33) > Cu^{2+} (1.190) > Fe^{2+} (1.83) > Zn^{2+} (1.65). This implies the fact that the higher the ion's electronegativity, the higher the attraction for its electrons and the attraction becomes stronger to the negative charge of the biomass ligands (Lezcano et al. 2010). Furthermore, the separation factor, R_L, for the metal ions falls within the range of $0 < R_L < 1$ (Table 2), suggesting that biosorption of the experimental cations is favorable at all the concentrations investigated (Weber and Chakravorti

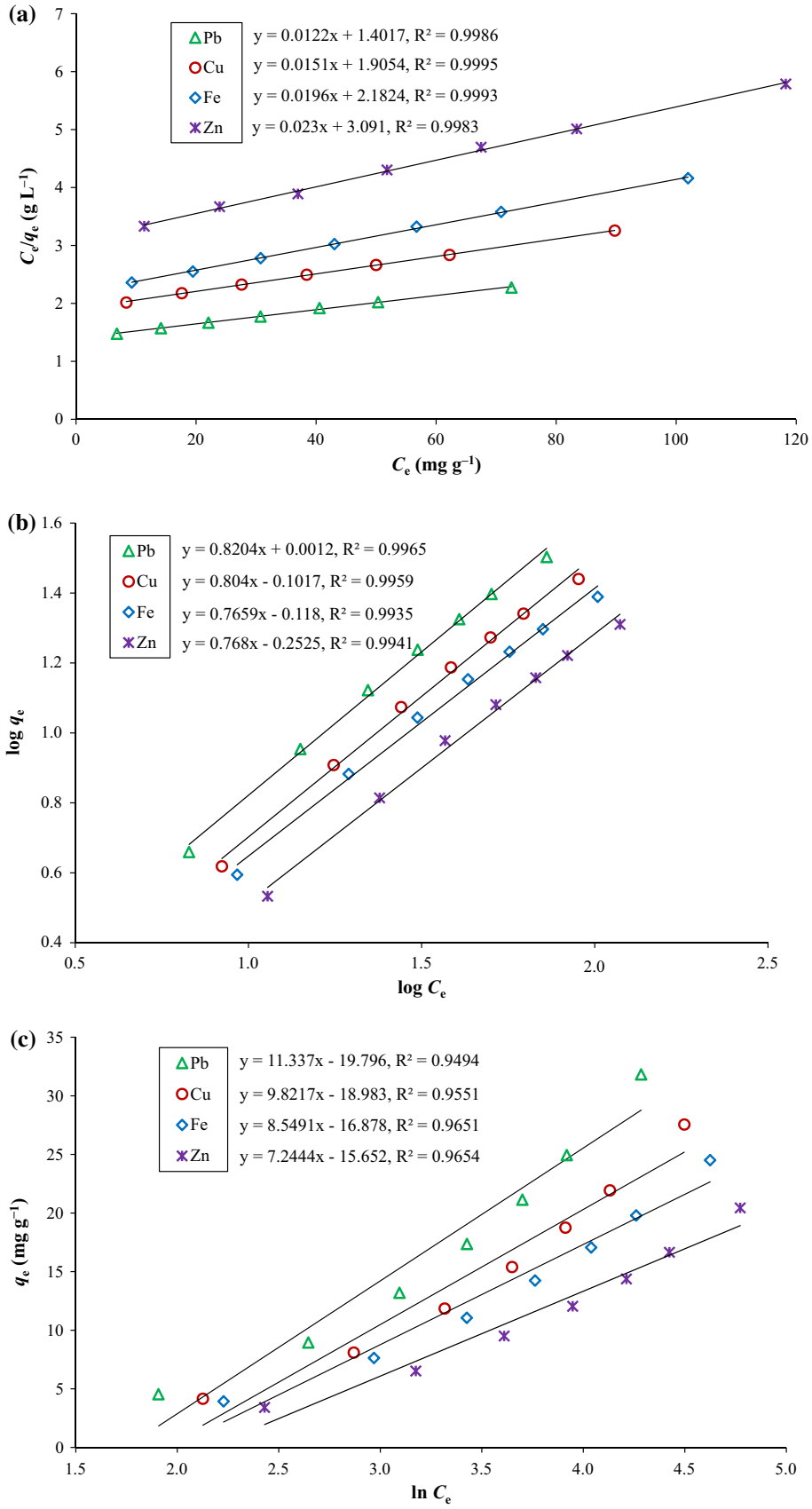

Fig. 2 Linearized biosorption isotherm models for the metal ions onto *E. denticulatum*: **a** Langmuir, **b** Freundlich and **c** Temkin models

Table 3 Isotherm model parameters for biosorption of the metal ions onto *E. denticulatum* dried biomass

Model	Parameter	Metal ions			
		Pb^{2+}	Cu^{2+}	Fe^{2+}	Zn^{2+}
Langmuir	q_m (mg g^{-1})	81.97	66.23	51.02	43.48
	K_L (L mg^{-1})	0.0087	0.0079	0.009	0.0074
	R_L	0.82–0.36	0.83–0.39	0.82–0.36	0.84–0.40
	R^2	0.999	0.999	0.999	0.998
Freundlich	K_F (mg g^{-1}) (L $mg^{-1})^{1/n}$	1.028	0.791	0.762	0.559
	n	1.219	1.244	1.306	1.302
	R^2	0.997	0.996	0.994	0.994
Temkin	q_m (mg g^{-1})	11.34	9.82	8.55	7.24
	A_T (L mg^{-1})	0.174	0.144	0.139	0.115
	b_T (kJ mol^{-1})	218.539	252.255	289.805	341.998
	R^2	0.949	0.955	0.965	0.965
Dubinin–Radushkevich	q_m (mg g^{-1})	20.95	18.46	16.81	14.2
	B_D (mol^2 kJ^{-2})	14.105	20.752	24.479	35.33
	R^2	0.795	0.797	0.807	0.808
	E (kJ mol^{-1})	0.188	0.155	0.143	0.119

1974). Hence, the *E. denticulatum* is a suitable biosorbent for the sorption of the experimental metal ions from aqueous solutions.

Freundlich isotherm model

The linearized Freundlich isotherm model (Fig. 2b) suggests that the biosorption of the metal ions moderately followed the Freundlich model ($R^2 \geq 0.99$). The magnitude of Freundlich constant, K_F (Table 3), suggests that the sorption capacity of the experimental metal ions was in the order of $Pb^{2+} > Cu^{2+} > Fe^{2+} > Zn^{2+}$. The values of $n > 1.0$ (Table 3) suggest the heterogeneity of the biomass surface, and the metal ions are favorably and intensively biosorbed by the biomass under the experimental conditions. Moreover, the applicability of both the Langmuir and Freundlich models ($R^2 \geq 0.99$) to the equilibrium biosorption data indicates both homogeneous and heterogeneous distribution of active sites on the biomass surface. Similar observations have been reported earlier for biosorption of metal ions by seaweeds (Plaza Cazón et al. 2013; Yalçın 2014).

Temkin isotherm model

The Temkin isotherm plots (Fig. 2c) and parameters (Table 3) indicate that the model does not fit the experimental data well for describing the metal ions biosorption ($R^2 \leq 0.97$). The Temkin adsorption potential, A_T (L mg^{-1}), was found in the order of $Pb^{2+} > Cu^{2+} > Fe^{2+} > Zn^{2+}$, indicating a lower sorbent-metal ion potential for Zn^{2+} probably due to its small ionic radius. The higher value of the Temkin constant, b_T (kJ mol^{-1}), for the metal ions (218.54–342.00) indicates the existence of a very strong bond between the metal ions and the biosorbent surface (Karim et al. 2012).

D–R isotherm model

The isotherm parameters (Table 3) indicate that the D–R model does not fit the experimental data well for describing the metal ions biosorption ($R^2 \approx 0.80$), suggesting the involvement of metal sorption mechanism other than van der Waals force (Basha et al. 2008). The mean biosorption energy, B_D (mol^2 kJ^{-2}), was found in the order of $Pb^{2+} < Cu^{2+} < Fe^{2+} < Zn^{2+}$, which indicates that the higher the electronegativity of metals, the lower the mean biosorption energy. The mean free energy of biosorption, E (kJ mol^{-1}), of the D–R isotherm model was found in the range of 0.119–0.188, suggesting physisorption nature of the sorption process (Dubinin 1960). Similar reports have been reported for metal biosorption by seaweed (Yalçın 2014) and modified orange peel (Lasheen et al. 2012). The positive values of E indicate the endothermic nature of the sorption process (Lasheen et al. 2012; Yalçın 2014). Furthermore, the values of E (<16 kJ mol^{-1}) suggest that the mechanism of the ion exchange process is film diffusion controlled (Boyd and Soldano 1953).

Competitive adsorption

Competitive adsorption of the metal ions under quaternary system shows the adsorption preference of $Pb^{2+} > Cu^{2+} > Fe^{2+} > Zn^{2+}$ with the rate of metal removal as

92.59, 92.33, 73.80 and 68.08 %, respectively. The results suggest that the potentiality of the adsorbent in the quaternary system remains the same as that in the single-metal system, which proves its unique adsorption quality.

Kinetic studies

Kinetic sorption mechanisms of the metal ions onto the biomass were evaluated using four kinetic models (pseudo-first-order, pseudo-second-order, Elovich and intraparticle diffusion). Results of the experimental data are represented in Table 4.

Pseudo-first-order kinetic studies

The regression coefficients of the pseudo-second-order model for the sorption of the heavy metal ions (Fig. 3a) were satisfactory ($R^2 = 0.98$–0.99), but the difference between the experimental values, $q_{e,exp}$, was higher than the modeled values, $q_{e,calc}$ (Table 4). It refers the fact that both the metal ions and adsorbent were involved in the adsorption process (Meitei and Prasad 2014). However, regression coefficients suggest that the pseudo-first-order model is suitable to explain the kinetic sorption of the experimental metal ions onto the biomass over the range of experimental time and metal ion concentrations.

Pseudo-second-order kinetic model

The regression coefficient of the linearized pseudo-second-order kinetic model (Fig. 3b; Table 4) was higher ($R^2 > 0.99$) than the other models, and the experimental $q_{e,exp}$ values matched well with the calculated data (Table 4) supporting the best fit of the model. Hence, chemisorption is the rate-limiting step which involves valence forces through the sharing or exchange of electrons between the metal ions and different functional groups in the sorbent (Plaza Cazón et al. 2013; Rathod et al. 2014).

The pseudo-second-order rate constant, k_2 (g mg^{-1} min^{-1}), was found in the order of $Pb^{2+} > Cu^{2+} > Fe^{2+} > Zn^{2+}$, which are in the order of maximum sorption capacity. The lower values of k_2 (0.0269–0.0867 g mg^{-1} min^{-1}) suggest that the metal ions uptake onto the sorbent from aqueous solution was more rapid and favorable. A fast initial uptake rate, h, was observed within the first 30 min where more than 75 % of the total metal adsorption occurred (data not shown here), followed by a slower uptake rate toward the point of equilibrium ($\sim$120 min). Similar observation was reported earlier in the literature (Arshadi et al. 2014; Meitei and Prasad, 2014). This phenomenon supports that the diffusion is the rate-controlling step in the sorption process (Plaza Cazón et al. 2013). The half-adsorption time $t_{1/2}$ (min) indicates high affinity between the molecules of the biomass and the metal ions.

Elovich kinetic model

The parameters of the Elovich kinetic model are given in Table 4. The Elovich kinetic model (Fig. 3c) does not support well fit of the model ($R^2 = 0.96$–0.98). Moreover, the lower values of the Elovich constants α (mg g^{-1} min^{-1}) and β (g mg^{-1}) indicate a slower rate of chemisorption

Table 4 Kinetic model parameters for biosorption of the metal ions onto *E. denticulatum* dried biomass

Model	Parameter	Metal ions			
		Pb^{2+}	Cu^{2+}	Fe^{2+}	Zn^{2+}
	$q_{e,exp}$ (mg g^{-1})	2.311	1.709	1.548	1.153
Pseudo-first-order	k_1 (min^{-1})	0.0283	0.0263	0.0302	0.0297
	$q_{e,calc}$ (mg g^{-1})	1.52	0.88	0.92	0.59
	R^2	0.995	0.981	0.991	0.975
Pseudo-second-order	k_2 (g mg^{-1} min^{-1})	0.0269	0.0542	0.052	0.0867
	$q_{e,calc}$ (mg g^{-1})	2.54	1.81	1.67	1.22
	h (mg g^{-1} min^{-1})	0.173	0.177	0.145	0.13
	$t_{1/2}$ (min)	14.67	10.22	11.51	9.42
	R^2	1	0.999	0.999	0.999
Elovich	α (mg g^{-1} min^{-1})	4.51E − 01	7.35E − 01	4.92E − 01	5.80E − 01
	β (g mg^{-1})	1.998	3.292	3.347	4.963
	R^2	0.979	0.972	0.974	0.962
Intraparticle diffusion	k_d (mg g^{-1} min$^{-0.5}$)	0.1465	0.0887	0.0946	0.0629
	C (mg g^{-1})	0.9151	0.8678	0.6884	0.5903
	R^2	0.990	0.970	0.977	0.963
Boyd	D_i (cm^2 s^{-1})	4.07E−06	5.84E−06	5.18E−06	6.34E−06
	R^2	0.995	0.981	0.991	0.975

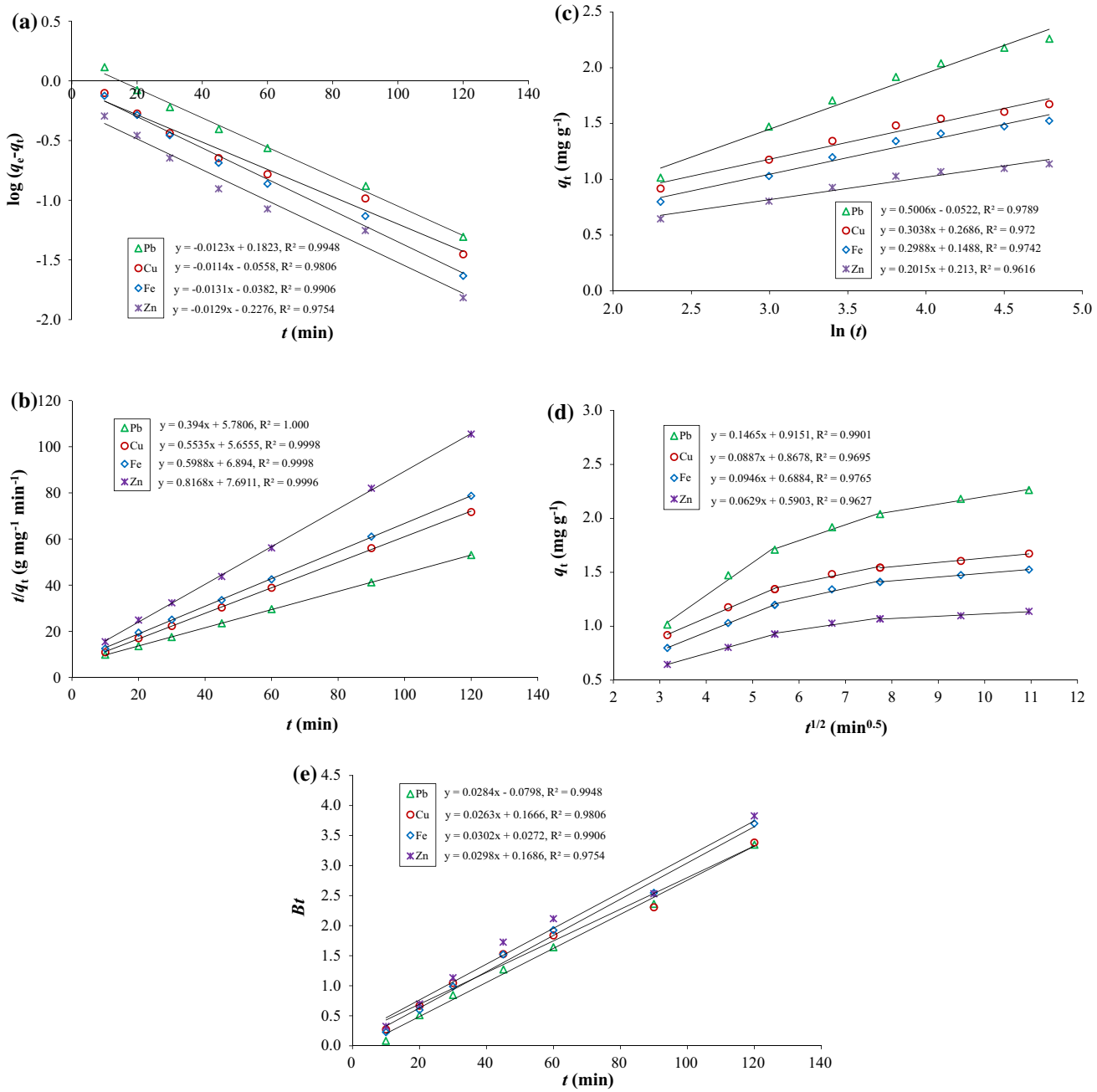

Fig. 3 Linearized kinetic models for the metal ions onto *E. denticulatum*: **a** pseudo-second-order, **b** pseudo-second-order, **c** Elovich, **d** intraparticle diffusion and **e** Boyd models

onto the biosorbent surface, which is in well agreement with the earlier report in the literature (Lasheen et al. 2012).

Intraparticle diffusion model

The nonlinear regression data of q_t versus $t^{0.5}$ plots (Fig. 3d) suggest that adsorption occurred in three phases: surface diffusion (initial linear portion), intraparticle diffusion (second linear portion) and final equilibrium stage (third section). Apparently, intraparticle diffusion plays a significant role in the uptake of Pb^{2+} ($R^2 \geq 0.99$). The intercept, *C,* in the second portion is indicative of the thickness of the boundary layer. The larger the intercept value, the greater is the boundary layer effect (Maksin et al. 2012; Rathod et al. 2014). However, the plots did not pass through the origin ($C > 0$) in any of the cases (Fig. 3d), suggesting that intraparticle diffusion was not the only rate-

controlling step (Maksin et al. 2012; Rathod et al. 2014), and external mass transfer had also played an important role in the metal ions sorption by the biomass.

Due to the multilinearity of the mass transfer model, Boyd model was tried to evaluate the actual rate-controlling step involved in the adsorption process. The Boyd plots of *Bt* versus *t* are linear ($R^2 \geq 0.98$) but do not pass through the origin (Fig. 3e), indicating the external mass transport (film diffusion)-controlled mechanism (Foo and Hameed 2013).

Thermodynamic study

The values of the thermodynamic parameters are given in Table 5, and the linearized van't Hoff plots of ln (K_{eq}) versus $1/T$ are represented in Fig. 4. The negative values of Gibbs free energy ($\Delta G°$) indicate spontaneous and feasible thermodynamic process (Gibbs 1873). Moreover, the increase in negative $\Delta G°$ values with an increase in temperature indicates an increased feasibility of adsorption at higher temperature (Massocatto et al. 2013; Meitei and Prasad 2014; Yalçın 2014).

The positive values of enthalpy change, $\Delta H°$ (Table 5), suggest the endothermic nature of the metal adsorption process (Meitei and Prasad 2014; Yalçın 2014). Based on the positive values of $\Delta H°$, it can be presumed that the biosorption process took place physically for the metal ions. This was also supported by the D–R isotherm results with the E values (<8 kJ mol^{-1}) of the metal ions (Table 3). Further, positive values of entropy change, $\Delta S°$ (Table 4), are suggestive of increased randomness at the solid–solution interface during the biosorption process of the metal ions on the active sites of the biosorbent (Massocatto et al. 2013).

Error function analysis

In the real world, data samples from each experiment in a series of experiments differ due to measurement error affecting data precision. This requires ensuring accurate measurement results, and statistical error function is the measure to compensate data errors (Leo 1994). Therefore, the isotherm and kinetic data were analyzed using nine error functions in order to test the fitness of the models.

Table 5 Thermodynamic parameters for biosorption of the metal ions onto *E. denticulatum* dried biomass

Metal ions	$\Delta H°$ (kJ mol^{-1})	$\Delta S°$ (kJ mol^{-1} K^{-1})	$\Delta G°$ (kJ mol^{-1})				R^2
			298 °K	303 °K	313 °K	323 °K	
Pb^{2+}	21.0777	77.8997	−2.1365	−2.526	−45.4603	−46.239	0.999
Cu^{2+}	4.3879	9.0598	−7.0877	−7.133	−7.2236	−7.3142	0.999
Fe^{2+}	7.2155	16.401	−12.103	−12.185	−12.349	−12.513	0.999
Zn^{2+}	7.2791	14.2036	−11.5118	−11.5828	−11.7248	−11.867	0.999

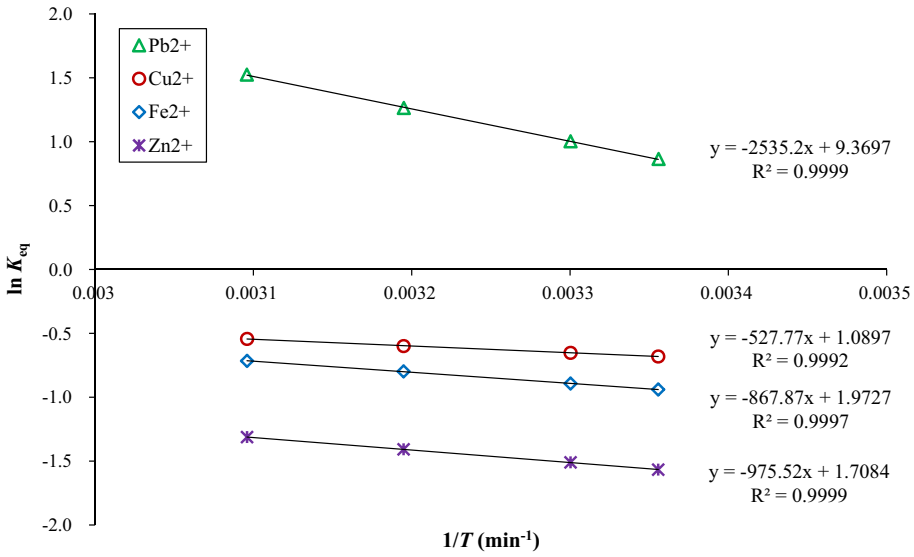

Fig. 4 Linearized van't Hoff plots of the thermodynamic data

Table 6 Error functions of the isotherm models for biosorption of the metal ions onto *E. denticulatum* dried biomass

Metal	Model	SSE	ARE	HYBRID	EABS	MPSD	r^2	χ^2	Δq (%)	RMSE
Pb^{2+}	Langmuir	0.08045	0.34969	0.48957	0.46448	2.70399	0.99985	0.00362	0.55617	0.12684
	Freundlich	74.2123	13.0165	18.2230	17.5463	81.2711	0.89962	2.76529	16.3228	3.85259
	Temkin	26.9412	16.4426	23.0196	12.1975	72.8546	0.94941	5.02898	26.5522	2.32126
	D–R	2003.41	80.8229	113.152	103.095	418.613	0.43148	673.742	87.6883	20.0170
Cu^{2+}	Langmuir	0.01218	0.31126	0.43576	0.26736	1.31570	0.99997	0.00087	0.39701	0.04935
	Freundlich	4.15329	3.32669	4.65737	3.62189	19.1329	0.99068	0.17619	4.22402	0.91140
	Temkin	17.6880	15.1352	21.1893	9.96188	63.3376	0.95514	3.42383	24.2725	1.88085
	D–R	1503.59	79.5718	111.400	89.6965	387.593	0.43367	528.143	86.3560	17.3412
Fe^{2+}	Langmuir	0.04282	0.35648	0.49907	0.39221	2.17585	0.99986	0.00236	0.49017	0.09254
	Freundlich	4.20453	4.11499	5.76099	3.88024	20.9746	0.98801	0.21261	5.12686	0.91701
	Temkin	10.6125	12.5792	17.6109	7.71481	50.8811	0.96509	1.91343	20.0579	1.45688
	D–R	1200.69	78.7104	110.195	80.7437	365.464	0.43734	436.061	85.4187	15.4964
Zn^{2+}	Langmuir	0.05409	0.67130	0.93982	0.50002	3.00013	0.99974	0.00450	0.84341	0.10401
	Freundlich	2.60404	3.70180	5.18253	2.98267	18.1186	0.98905	0.15987	4.77922	0.72167
	Temkin	7.19822	12.2409	17.1373	6.43082	45.4309	0.96543	1.47884	19.2448	1.19985
	D–R	813.879	76.8444	107.582	66.5981	328.203	0.43844	315.315	83.4309	12.7584

Lower value of SSE, ARE, HYBRID, EABS, MPSD, χ^2, Δq (%), RMSE, and higher value of r^2 represent the best fit of the model.

The error functions of the isotherm data (Table 6) suggest that the Langmuir model provides the best fit to the experimental data for biosorption of the metal ions. The Freundlich model provides moderate fit to the experimental data for adsorption of the metal ions. The regression coefficient ($R^2 = 0.997$) suggests that Pb^{2+} adsorption follows the Freundlich model moderately (Table 3), while the error functions (Table 6) suggest that the Temkin model provides moderate fit for adsorption of Pb^{2+}.

The regression coefficient of the pseudo-first-order kinetic models (Table 4) shows a moderate fit of the model ($R^2 \geq 0.98$) for biosorption of the metal ions. But the error functions (Table 7) do not support the good fit of the data. The regression coefficient of the pseudo-second-order model (Table 4) suggests the best fit of the experimental data. In

Table 7 Error functions of the kinetic models for biosorption of the metal ions onto *E. denticulatum* dried biomass

Metal	Model	SSE	ARE	HYBRID	EABS	MPSD	r^2	χ^2	Δq (%)	RMSE
Pb^{2+}	Pseudo-first-order	2.01658	28.3337	39.6672	3.35155	49.2641	0.23890	1.30856	37.1805	0.63507
	Pseudo-second-order	0.00030	0.35875	0.50225	0.03327	0.71577	0.99974	0.00025	0.61389	0.00778
	Elovich	0.02442	3.36610	4.71253	0.37880	5.62122	0.97893	0.01531	4.37289	0.06989
	Intraparticle diffusion	0.00055	0.67362	2.02087	0.03830	1.70023	0.99014	0.00029	0.87177	0.02348
Cu^{2+}	Pseudo-first-order	2.69793	37.5223	52.53117	3.91350	59.3107	0.43865	3.32620	43.8855	0.73457
	Pseudo-second-order	0.00148	0.98709	1.38193	0.08432	1.60654	0.99670	0.00130	1.40463	0.01719
	Elovich	3.99150	52.0053	72.8075	5.13918	73.8060	0.48829	5.84831	56.3552	0.89348
	Intraparticle diffusion	0.00064	0.93736	2.81208	0.04118	2.08292	0.96946	0.00044	1.21433	0.02529
Fe^{2+}	Pseudo-first-order	1.54854	32.2360	45.1304	2.97616	47.2419	0.38211	1.80582	37.0041	0.55651
	Pseudo-second-order	0.00180	1.23239	1.72534	0.09132	1.90117	0.99573	0.00180	1.76629	0.01897
	Elovich	0.01069	2.95342	4.13479	0.25338	4.12265	0.97423	0.00850	3.45154	0.04624
	Intraparticle diffusion	0.00056	0.96910	2.90729	0.03847	2.04381	0.97646	0.00042	1.25345	0.02359
Zn^{2+}	Pseudo-first-order	1.24257	36.2325	50.7255	2.59402	48.6164	0.44319	2.36047	43.4261	0.49851
	Pseudo-second-order	0.00155	1.44357	2.02100	0.08787	1.92304	0.99194	0.00183	1.94358	0.01761
	Elovich	0.00735	3.24218	4.53905	0.21436	3.90733	0.96158	0.00767	3.71240	0.03833
	Intraparticle diffusion	0.00040	1.07228	0.64337	0.03259	1.96727	0.96276	0.00039	1.37865	0.01987

Table 8 FTIR assignment in the cell wall of *E. denticulatum* dried biomass

Functional groups (γ cm^{-1})	*E. denticulatum* dried biomass, raw and after metal adsorption				
	Raw	Pb^{2+}	Cu^{2+}	Fe^{2+}	Zn^{2+}
γ O–H and γ N–H	3342.2	3322.7	3327.3	3289	3324.7
γ C–H	2925.1	2919.5	2918.8	2921	2920.0
γ C=O	1637.9	1639.2	1638.3	1637.8	1641.4
γ $-SO_3^-$	1373.3	1370.1	1366.8	1367.5	1370.3
γ C=O	1215.0	1228.6	1229.3	1231.1	1228.1
γ $-SO_3^-$	1154.4	1155.0	1153.8	1154.1	1154.6
γ –C–O	1123.9	–	–	–	–
γ C–O	1033.2	1021.6	1022.1	1022.7	1023.9
γ S–O	923.6	928.5	929.2	–	929.9
γ S=O	844.5	–	–	–	–

contrast to this, the error functions (Table 7) support moderately (for Cu^{2+}, Fe^{2+} and Zn^{2+}) and strongly (for Pb^{2+}) fit of the model, and vice versa for the intraparticle diffusion model.

It is, however, observed that the isotherm and kinetic models in describing the metal ions biosorption onto the biosorbent are metal ions dependent under the experimental conditions. Nonetheless, it is strongly suggested that the regression coefficient (R^2) is not an appropriate method in characterizing the best fit of isotherm and kinetic models; rather, some forms of error analysis could be a better criterion for avoiding data errors.

Fourier transform infrared spectroscopy (FTIR)

The spectra of FTIR analysis show a number of functional groups, such as amine, aliphatic, carboxylate, carboxyl, sulfonate and ether groups in the cell wall of *E. denticulatum* (Table 8; Fig. 5).

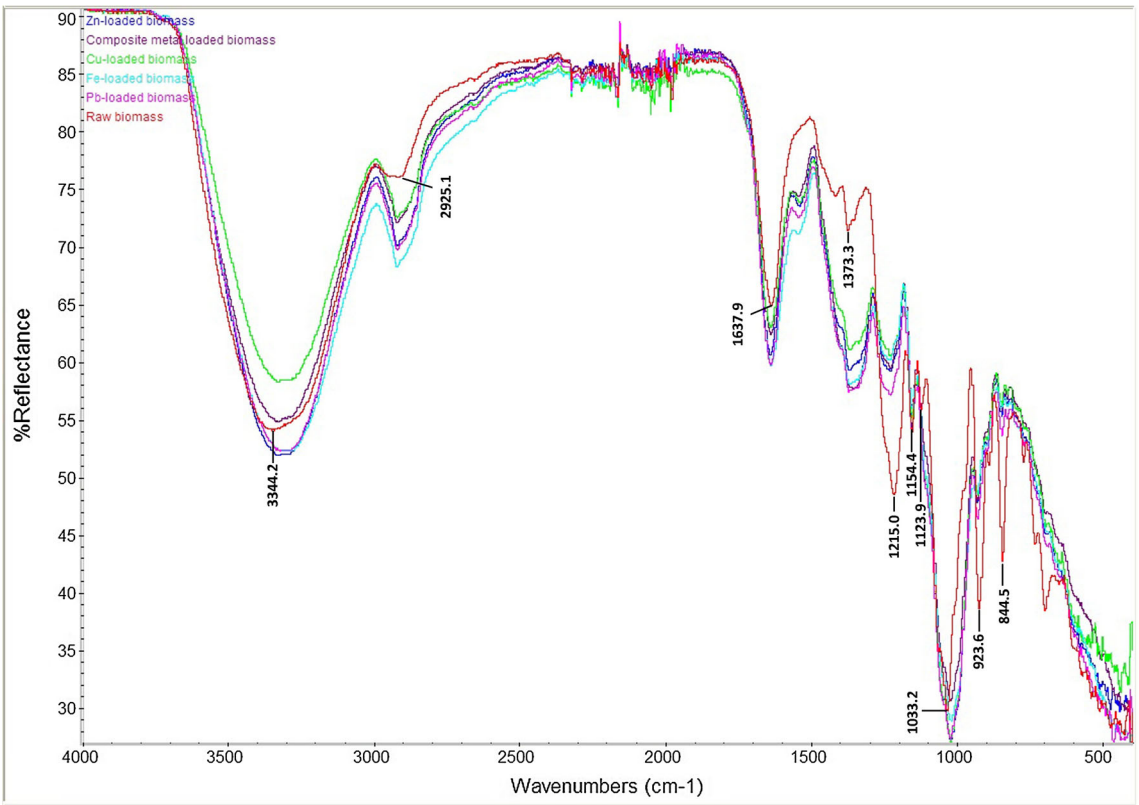

Fig. 5 FTIR spectra of the dried biomass of *E. denticulatum* before and after absorption of the metal ions

The strong broad peak observed at 3342.2 cm^{-1} (raw biomass) corresponds to O–H group from cellulose and N–H groups from proteins in the seaweed (Bhatnagar et al. 2012). This band shifted to a lower wave number after metal binding, suggesting their contribution in the experimental metal ions biosorption.

The peak at 2917.1 cm^{-1} (raw biomass) corresponds to asymmetric C–H stretching vibrations of aliphatic groups and shifts to a lower wave number after metal binding suggesting that the aliphatic groups were responsible for the heavy metal adsorption (Nessim et al. 2011).

The two strong peaks at 1637.9 and 1215.0 cm^{-1} (raw biomass) can be attributed to C=O stretching vibration of carboxylate groups (Plaza Cazón et al. 2013; Yalçın 2014). These peaks shifted significantly after metal binding which suggest that carboxylic groups played an important role in the biosorption of the experimental heavy metals through complexation mechanism (Rathod et al. 2014; Yalçın 2014).

Absorbance peaks at 1373.3 and 1154.4 cm^{-1} (raw biomass) can be assigned due to asymmetric and symmetric stretching of $–SO_3^-$ bonds of sulfonic acid, respectively (Yalçın 2014). Some degree of horizontal shift of these bands after metal binding indicated that chelating complexes were formed during adsorption of the experimental metal ions (Plaza Cazón et al. 2013).

The presence of peak at 1033.2 cm^{-1} (raw biomass) is attributed to C–O stretching vibration of carboxyl groups (Plaza Cazón et al. 2013) that shifted to a significant lower peak after metal binding, which might be due to the chelating complexation (bidentate complex) of the experimental metal ions to the carboxylic groups (Pennesi et al. 2012).

Absorbance peaks at 923.6 and 844.5 cm^{-1} (raw biomass) correspond to S–O stretching (Plaza Cazón et al. 2013) and S=O stretching bands of sulfonate groups (Yalçın 2014). These bands decreased and disappeared, respectively, after metal binding which was typical of complexation of the sulfonate groups by dative coordination with the experimental metal ions (Yalçın 2014; Yalçın et al. 2012).

Absorbance peak at 1123.9 cm^{-1} (the raw biomass) is attributed to the –C–O stretching of ether groups (Sheng et al. 2004) that disappeared after metal binding suggesting that the ether groups were also responsible for the biosorption of the experimental metal ions.

Conclusion

In the present study, we evaluated biosorption quality of four heavy metal ions like Pb^{2+}, Cu^{2+}, Fe^{2+} and Zn^{2+} onto the dried biomass of the red seaweed, *E. denticulatum,* from Malaysia. The FTIR study revealed the presence of amine, aliphatic, carboxylate, carboxyl, sulfonate and ether groups in the cell wall matrix of the biomass that was involved in the adsorption of the metal ions. The solution pH, contact time, temperature and initial metal ion concentration have a significant effect on the biosorption efficiency.

Heavy metal biosorption process onto the biosorbent representing both homogeneous and heterogeneous active sites was the complex one involving both physisorption and chemisorption and was feasible, spontaneous and endothermic in nature. Error function analysis, an accurate measurement of the experimental data, shows that the adsorption isotherm data for all the experimental metal ions fitted well with the Langmuir model followed by the Freundlich model (for Cu^{2+}, Fe^{2+} and Zn^{2+}) and the Temkin model (for Pb^{2+}). Kinetic data for the metal ions (Cu^{2+}, Fe^{2+} and Zn^{2+}) could be best described by the intraparticle diffusion model followed by the pseudo-second-order model, and vice versa for Pb^{2+} biosorption. We strongly suggest analysis of error functions as a better criterion in order to characterize isotherm and kinetic models describing adsorptive behavior of a typical adsorbent using linear method.

The results provide the potential of *E. denticulatum* as a new, low-cost and promising biosorbent for the removal of Pb^{2+}, Cu^{2+}, Fe^{2+} and Zn^{2+} from aqueous solutions. It can pave a way toward sustainable utilization of the dried *E. denticulatum* biomass for the restoration of industrial wastewater contaminated with heavy metal ions. However, further study is warranted to evaluate the feasibility of the biosorbent for removal of heavy metals from the real environment.

Acknowledgments The authors greatly acknowledge the financial support of the AIMST University (Grant Number: AURGC/1/FAS/2013) for the research.

References

Al-Homaidan AA, Al-Houri HJ, Al-Hazzani AA, Elgaaly G, Moubayed NMS (2014) Biosorption of copper ions from aqueous solutions by *Spirulina platensis* biomass. Arabian J Chem 7:57–62. doi:10.1016/j.arabjc.2013.05.022

Arshadi M, Amiri MJ, Mousavi S (2014) Kinetic, equilibrium and thermodynamic investigations of Ni(II), Cd(II), Cu(II) and Co(II) adsorption on barley straw ash. Water Resour Ind 6:1–17. doi:10.1016/j.wri.2014.06.001

Basha S, Murthy ZVP, Jha B (2008) Isotherm modeling for biosorption of Cu(II) and Ni(II) from wastewater onto brown seaweed, *Cystoseira indica*. AIChE J 54:3291–3302. doi:10.1002/aic.11606

Basha S, Jaiswar S, Jha B (2010) On the biosorption, by brown seaweed, Lobophora variegata, of Ni(II) from aqueous solutions: equilibrium and thermodynamic studies. Biodegradation 21:661–680. doi:10.1007/s10532-010-9333-4

Bhatnagar A, Vilar VJP, Ferreira C, Botelho CMS, Boaventura RAR (2012) Optimization of nickel biosorption by chemically modified brown macroalgae (*Pelvetia canaliculata*). Chem Eng J 193–194:256–266. doi:10.1016/j.cej.2012.04.037

Bilal M, Shah JA, Ashfaq T, Gardazi SMH, Tahir AA, Pervez A et al (2013) Waste biomass adsorbents for copper removal from industrial wastewater—a review. J Hazard Mater 263:322–333. doi:10.1016/j.jhazmat.2013.07.071

Boyd GE, Soldano BA (1953) Self-diffusion of cations in and through sulfonated polystyrene cation-exchange polymers. J Am Chem Soc 75:6091–6099. doi:10.1021/ja01120a001

Boyd GE, Adamson AW, Myers LS (1947) The Exchange adsorption of ions from aqueous solutions by organic zeolites. II. Kinetics1. J Am Chem Soc 69:2836–2848. doi:10.1021/ja01203a066

Carpenter KE, Niem VH (1998) FAO species identification guide for fishery purposes. The living marine resources of the Western Central Pacific. Volume 1. Seaweeds, corals, bivalves and gastropods. FAO, Rome

Chan LS, Cheung WH, Allen SJ, McKay G (2012) Error analysis of adsorption isotherm models for acid dyes onto bamboo derived activated carbon. Chin J Chem Eng 20:535–542. doi:10.1016/S1004-9541(11)60216-4

Chien SH, Clayton WR (1980) Application of elovich equation to the kinetics of phosphate release and sorption in soils. Soil Sci Soc Am J 44:265–268. doi:10.2136/sssaj1980.03615995004400020013x

Chowdhury P, Elkamel A, Ray AK (2015) Photocatalytic processes for the removal of toxic metal ions. In: Sharma SK (ed) Heavy metals in water: presence, removal and safety. The Royal Society of Chemistry, UK, pp 25–43

de Souza FB, de Souza SMAG, de Souza AAU, Costa CE, Botelho CS, Vilar VP, Boaventura RR (2013) Modeling of trivalent chromium speciation in binding sites of marine macroalgae *Sargassum cymosum*. Clean Technol Environ Policy 15:987–997. doi:10.1007/s10098-012-0573-3

Dubinin MM (1960) The potential theory of adsorption of gases and vapors for adsorbents with energetically nonuniform surfaces. Chem Rev 60:235–241. doi:10.1021/cr60204a006

Dubinin MM, Radushkevich LV (1947) Equation of the characteristic curve of the activated charcoal. Chem Zentralbl 1:875–890

Foo KY, Hameed BH (2013) Utilization of oil palm biodiesel solid residue as renewable sources for preparation of granular activated carbon by microwave induced KOH activation. Bioresour Technol 130:696–702. doi:10.1016/j.biortech.2012.11.146

Freile-Pelegrín Y, Robledo D, Azamar JA (2006) Carrageenan of *Eucheuma isiforme* (Solieriaceae, Rhodophyta) from Yucatán, Mexico. I. Effect of extraction conditions. Bot Mar 49:65–71. doi:10.1515/BOT.2006.008

Freundlich HMF (1906) Über die adsorption in lösungen. Z Phys Chem Leipz 57:385–470

Gautam RK, Sharma SK, Mahiya S, Chattopadhyaya MC (2015) Contamination of heavy metals in aquatic media: transport, toxicity and technologies for remediation. In: Sharma SK (ed) Heavy metals in water: presence, removal and safety. The Royal Society of Chemistry, UK, pp 1–24

Gibbs JW (1873) A method of geometrical representation of the thermodynamic properties of substances by means of surfaces. Trans Conn Acad Arts Sci 2:382–404

Grassi M, Kaykioglu G, Belgiorno V, Lofrano G (2012) Removal of emerging contaminants from water and wastewater by adsorption process. In: Lofrano G (ed) Emerging compounds removal from wastewater. Springer, Netherlands, pp 15–37

Gupta SS, Bhattacharyya KG (2011) Kinetics of adsorption of metal ions on inorganic materials: a review. Adv Colloid Interface Sci 162:39–58. doi:10.1016/j.cis.2010.12.004

He J, Chen JP (2014) A comprehensive review on biosorption of heavy metals by algal biomass: materials, performances, chemistry, and modeling simulation tools. Bioresour Technol 160:67–78. doi:10.1016/j.biortech.2014.01.068

He J, Hong S, Zhang L, Gan F, Ho YS (2010) Equilibrium and thermodynamic parameters of adsorption of methylene blue onto rectorite. Fresenius Environ Bull 19:2651–2656

Ho YS (1995) Adsorption of heavy metals from waste streams by peat. Dissertation, University of Birmingham

Ho Y-S (2004) Selection of optimum sorption isotherm. Carbon 42:2115–2116. doi:10.1016/j.carbon.2004.03.019

Ho YS, Ofomaja AE (2006) Pseudo-second-order model for lead ion sorption from aqueous solutions onto palm kernel fiber. J Hazard Mater 129:137–142. doi:10.1016/j.jhazmat.2005.08.020

Hobson JP (1969) Physical adsorption isotherms extending from ultrahigh vacuum to vapor pressure. J Phys Chem 73:2720–2727. doi:10.1021/j100842a045

Ibrahim WM (2011) Biosorption of heavy metal ions from aqueous solution by red macroalgae. J Hazard Mater 192:1827–1835. doi:10.1016/j.jhazmat.2011.07.019

Karim AH, Jalil AA, Triwahyono S, Kamarudin NHN, Salleh NFM, Aziz MAA (2012) Adsorption of methylene blue from aqueous solution by mesostructured silica nanoparticles. In: Proceedings of the 5th international conference on postgraduate education (ICPE-5 2012), 18–19 December 2012, Universiti Technologi Malaysia, Malaysia

Kumar PS, Saravanan A, Rajan PS, Yashwanthraj M (2016) Nanoscale zero-valent iron-impregnated agricultural waste as an effective biosorbent for the removal of heavy metal ions from wastewater. Text Cloth Sustai 2:3. doi:10.1186/s40689-016-0014-5

Lagergren SY (1898) Zur Theorie der sogenannten Adsorption gelöster Stoffe. Kongl Svenska Vetensk Akad Handl 24:1–39

Langmuir I (1918) The adsorption of gases on plane surfaces of glass, mica and platinum. J Am Chem Soc 40:1361–1403. doi:10.1021/ja02242a004

Lasheen MR, Ammar NS, Ibrahim HS (2012) Adsorption/desorption of Cd(II), Cu(II) and Pb(II) using chemically modified orange peel: equilibrium and kinetic studies. Solid State Sci 14:202–210. doi:10.1016/j.solidstatesciences.2011.11.029

Leo WR (1994) Techniques for nuclear and particle physics experiments: a how-to approach, 2nd edn. Springer, Berlin, pp 81–113

Lezcano JM, González F, Ballester A, Blázquez ML, Muñoz JA, García-Balboa C (2010) Biosorption of Cd(II), Cu(II), Ni(II), Pb(II) and Zn(II) using different residual biomass. Chem Ecol 26:1–17. doi:10.1080/02757540903468102

Macek T, Mackova M (2011) Potential of biosorption technology. In: Kotrba P, Mackova M, Macek T (eds) Microbial biosorption of metals. Springer, Netherlands, pp 7–17

Maksin DD, Kljajević SO, Đolić MB, Marković JP, Ekmeščić BM, Onjia AE, Nastasović AB (2012) Kinetic modeling of heavy metal sorption by vinyl pyridine based copolymer. Hem Ind 66:795–804. doi:10.2298/HEMIND121002112M

Massocatto CL, Paschoal EC, Buzinaro N, Oliveria TF, Tarley CRT, Caetano J et al (2013) Preparation and evaluation of kinetics and thermodynamics studies of lead adsorption onto chemically modified banana peels. Desalin Water Treat 51:5682–5691. doi:10.1080/19443994.2013.770614

Meitei MD, Prasad MNV (2014) Adsorption of Cu (II), Mn(II) and Zn (II) by *Spirodela polyrhiza* (L.) Schleiden: equilibrium, kinetic and thermodynamic studies. Ecol Eng 71:308–317. doi:10.1016/j.ecoleng.2014.07.036

Ncibi MC, Altenor S, Seffen M, Brouers F, Gaspard S (2008) Modelling single compound adsorption onto porous and non-porous sorbents using a deformed Weibull exponential isotherm. Chem Eng J 145:196–202. doi:10.1016/j.cej.2008.04.001

Nessim RB, Bassiouny AR, Zaki HR, Moawad MN, Kandeel KM (2011) Biosorption of lead and cadmium using marine algae. Chem Ecol 27:579–594. doi:10.1080/02757540.2011.607439

Park D, Yun YS, Park J (2010) The past, present, and future trends of biosorption. Biotechnol Bioprocess Eng 15:86–102. doi:10.1007/s12257-009-0199-4

Pauling L (1960) The nature of the chemical bond: an introduction to modern structural chemistry, 3rd edn. Cornell University Press, Ithaca

Pennesi C, Totti C, Romagnoli T, Bianco B, De Michelis I, Beolchini F (2012) Marine macrophytes as effective lead biosorbents. Water Environ Res 84:9–16. doi:10.2175/106143011X12989211841296

Perales YJ, Leysa M (2012) Eucheuma denticulatom as potential biosorbent for lead nitrate, cadmium sulfide and zinc sulfate contaminated waters. Int Proc Chem Biol Environ Eng 45:117–120. doi:10.7763/IPCBEE.2012.V45.24

Plaza Cazón J, Viera M, Donati E, Guibal E (2013) Zinc and cadmium removal by biosorption on *Undaria pinnatifida* in batch and continuous processes. J Environ Manag 129:423–434. doi:10.1016/j.jenvman.2013.07.011

Plazinski W, Plazinska A (2012) Equilibrium and kinetic modeling of adsorption at solid/solution interface. In: Bhatnagar A (ed) Application of adsorbents for water pollution control. Bentham Science Publishers, The Netherlands, pp 32–80

Rathod M, Mody K, Basha S (2014) Efficient removal of phosphate from aqueous solutions by red seaweed, *Kappaphycus alvarezii*. J Clean Prod 84:484–493. doi:10.1016/j.jclepro.2014.03.064

Reichenberg D (1953) Properties of ion-exchange resins in relation to their structure. III. Kinetics of exchange. J Am Chem Soc 75:589–597. doi:10.1021/ja01099a022

Renaud S, Luong-Van J (2006) Seasonal variation in the chemical composition of tropical Australian marine macroalgae. J Appl Phycol 18:381–387. doi:10.1007/s10811-006-9034-x

Roginsky SZ, Zeldovich YB (1934) Die katalische Oxidation von Kohlenmonoxyd auf Mangandioxyd. Acta Physiochim USSR 1:554–594

Sarkar A, Bhagat J, Sarker S (2014) Evaluation of impairment of DNA in marine gastropod, *Morula granulata* as a biomarker of marine pollution. Ecotox Environ Safe 106:253–261. doi:10.1016/j.ecoenv.2014.04.023

Sheng PX, Ting YP, Chen JP, Hong L (2004) Sorption of lead, copper, cadmium, zinc, and nickel by marine algal biomass: characterization of biosorptive capacity and investigation of mechanisms. J Colloid Interface Sci 275:131–141. doi:10.1016/j.jcis.2004.01.036

Sherwood AR, Kurihara A, Conklin KY, Sauvage T, Presting GG (2010) The Hawaiian Rhodophyta Biodiversity Survey (2006-2010): a summary of principal findings. BMC Plant Biol 10:258. doi:10.1186/1471-2229-10-258

Sreńscek-Nazzal J, Narkiewicz U, Morawski AW, Wróbel RJ, Michalkiewicz B (2015) Comparison of optimized isotherm models and error functions for carbon dioxide adsorption on activated carbon. Pol J Chem Eng Data 60:3148–3158. doi:10.1021/acs.jced.5b00294

Su Y, Zhao B, Xiao W, Han R (2013) Adsorption behavior of light green anionic dye using cationic surfactant-modified wheat straw in batch and column mode. Environ Sci Pollut Res 20:5558–5568. doi:10.1007/s11356-013-1571-7

Subramanyam B, Das A (2014) Linearised and non-linearised isotherm models optimization analysis by error functions and statistical means. J Environ Health Sci Eng 12:92. doi:10.1186/2052-336X-12-92

Temkin MJ, Pyzhev V (1940) Recent modifications to Langmuir isotherms. Acta Physiochim USSR 12:217–222

Vijayaraghavan K, Padmesh TVN, Palanivelu K, Velan M (2006) Biosorption of nickel(II) ions onto *Sargassum wightii*: application of two-parameter and three-parameter isotherm models. J Hazard Mater 133:304–308. doi:10.1016/j.jhazmat.2005.10.016

Wang L, Zhang J, Zhao R, Li Y, Li C, Zhang C (2010) Adsorption of Pb(II) on activated carbon prepared from *Polygonum orientale* Linn.: kinetics, isotherms, pH, and ionic strength studies. Bioresour Technol 101:5808–5814. doi:10.1016/j.biortech.2010.02.099

Weber TW, Chakravorti RK (1974) Pore and solid diffusion models for fixed-bed adsorbers. AIChE J 20:228–238. doi:10.1002/aic.690200204

Weber WJ, Morris JC (1963) Kinetics of adsorption on carbon from solution. J Environ Eng ASCE 89:31–60

Yalçın S (2014) The mechanism of heavy metal biosorption on green marine macroalga *Enteromorpha linza*. CLEAN 42:251–259. doi:10.1002/clen.201200500

Yalçın S, Sezer S, Apak R (2012) Characterization and lead(II), cadmium(II), nickel(II) biosorption of dried marine brown macro algae *Cystoseira barbata*. Environ Sci Pollut Res 19:3118–3125. doi:10.1007/s11356-012-0807-2